DOI: 10.1534/genetics.110.120840

Tyrosinase Is the Modifier of Retinoschisis in Mice

Britt A. Johnson,*[,1,2] Brian S. Cole,*[,1] Eldon E. Geisert,[†] Sakae Ikeda* and Akihiro Ikeda*[,3]

Department of Medical Genetics, University of Wisconsin, Madison, Wisconsin 53706 and [†]Department of Ophthalmology, University of Tennessee College of Medicine, Memphis, Tennessee 38163

Manuscript received July 12, 2010
Accepted for publication September 21, 2010

ABSTRACT

X-linked retinoschisis (XLRS) is a form of macular degeneration with a juvenile onset. This disease is caused by mutations in the retinoschisin (*RS1*) gene. The major clinical pathologies of this disease include splitting of the retina (schisis) and a loss in synaptic transmission. Human XLRS patients display a broad range in phenotypic severity, even among family members with the same mutation. This variation suggests the existence of genetic modifiers that may contribute to disease severity. Previously, we reported the identification of a modifier locus, named *Mor1*, which affects severity of schisis in a mouse model of XLRS (the $Rs1^{tmgc1}$ mouse). Homozygosity for the protective AKR allele of *Mor1* restores cell adhesion in $Rs1^{tmgc1}$ mice. Here, we report our study to identify the *Mor1* gene. Through collecting recombinant mice followed by progeny testing, we have localized *Mor1* to a 4.4-Mb region on chromosome 7. In this genetic region, the AKR strain is known to carry a mutation in the tyrosinase (*Tyr*) gene. We observed that the schisis phenotype caused by the *Rs1* mutation is rescued by a *Tyr* mutation in the C57BL/6J genetic background, strongly suggesting that *Tyr* is the *Mor1* gene.

X-LINKED retinoschisis (XLRS) (OMIM 312700) is a juvenile form of macular degeneration with an incidence of 1 in 5000 to 1 in 25,000 male children (George *et al.* 1995). The major features of this disease include retinal and vitreous degeneration, reduced visual acuity, foveal schisis (splitting of the central retina), and a reduction in the electroretinogram (ERG) b-wave (reduced synaptic transmission in the retina) (Peachey *et al.* 1987; George *et al.* 1996; Retinoschisis Consortium 1998; Seiving 1998).

XLRS is caused by mutations in the retinoschisin (*RS1*) gene (Sauer *et al.* 1997). *RS1* transcription has been detected in the retina (Sauer *et al.* 1997), the pineal gland (Takada *et al.* 2006), and the uterus (Huopaniemi *et al.* 1999). In the retina, *RS1* is transcribed in the photoreceptor cells (Reid *et al.* 1999), bipolar cells (Molday *et al.* 2001), and ganglion cells (Takada *et al.* 2004). *RS1* encodes the 224-amino-acid protein, retinoschisin (RS1) (Sauer *et al.* 1997). RS1 contains an N-terminal leader sequence that is cleaved for secretion from the ER to the plasma membrane, an Rs1 domain, and a discoidin domain (Wu and Molday 2003). The discoidin domain is the most prominent feature of RS1, comprising >75% of the processed protein (Sauer *et al.* 1997). Discoidin domains are highly conserved across many species and are generally involved in cell–cell interactions and cell adhesion (Baumgartner *et al.* 1998). Recently, Na/K ATPase-SARM1 complex (Molday *et al.* 2007) and L-type voltage-gated calcium channels (Shi *et al.* 2009) were identified as binding partners of RS1.

One hundred seventy-one unique allelic variants of *RS1* mutations such as frameshifts, exon deletions, splice-site mutations, and nonsense/missense mutations have been identified to date (Retinoschisis Consortium 1998). A most recent study showed that the b/a-wave ratio of the XLRS patients determined by ERG is correlated with the severity of the misssense mutation (Sergeev *et al.* 2010). On the other hand, family members with the same RS1 mutation show significant variation in phenotypic severity (Eksandh *et al.* 2000; Pimenides *et al.* 2005). Lack of genotype–phenotype correlations and intrafamilial disease heterogeneity in theses families suggests the existence of genetic modifiers or differential susceptibility to environmental factors. These observations in the human population suggest that the severity of phenotypes in XLRS patients may be independently influenced by the nature of the mutation and genetic factors. However, the heterogeneous nature of human populations and the variability of possible environmental influences make it difficult to dissect out the genetic factors. Modifier screens in mouse models overcome these challenges by enabling the use of genetically homogenous populations and controlled environments.

Supporting information is available online at http://www.genetics.org/cgi/content/full/genetics.110.120840/DC1.

[1]These authors contributed equally to this work.

[2]*Present address:* Department of Neurology, University of California, San Francisco, CA 94143.

[3]*Corresponding author:* Department of Medical Genetics, University of Wisconsin, Room 5350 Genetics/Biotech, 425-G Henry Mall, Madison, WI 53706. E-mail: aikeda@wisc.edu

The *Rs1*^{tmgc1} mouse has been a valuable model for the study of XLRS. These mice contain a splice-site mutation in the murine *RS1* homolog, *Rs1*. (Jablonski *et al.* 2005a). The splice-site mutation causes aberrant splicing of *Rs1*. However, 30% of *Rs1* transcripts are still properly spliced in these mice (Johnson *et al.* 2008). *Rs1*^{tmgc1} mice have phenotypes similar to human XLRS patients such as a reduced ERG b-wave and schisis (Jablonski *et al.* 2005a; Johnson *et al.* 2006, 2008). Ectopic photoreceptor synapses and a reduced areal density of synaptic vesicles at the photoreceptor presynapse have also been reported and may account for some of the reduction in synaptic transmission in *Rs1*^{tmgc1} retina (Johnson *et al.* 2006).

Recently, we reported the identification of a modifier quantitative trait locus (QTL), named *Mor1* for **m**odifier **o**f ***R****s1* **1**, which affects the disease severity in *Rs1*^{tmgc1} mice (Johnson *et al.* 2008). Homozygosity for the protective allele of *Mor1*, derived from the AKR/J inbred mouse strain, restores cell adhesion in *Rs1*^{tmgc1} mutant mice. The genetic region of *Mor1* was localized between markers D7Mit279 and D7Mit237 on mouse chromosome (Chr) 7 (Johnson *et al.* 2008). The exact function of *Mor1* was still unknown. However, studies using fragment analysis have shown that *Mor1* is most likely not involved in the splicing of *Rs1* (Johnson *et al.* 2008).

In this study, we report positional cloning of *Mor1*, a modifier of *Rs1* on Chr 7, which restores cell adhesion in the retina of *Rs1*^{tmgc1} mice.

MATERIALS AND METHODS

Mice: All mouse procedures were performed in accordance with the Association for Research in Vision and Ophthalmology's statement for the use of animals in ophthalmic and vision research. 44TNJ (*Rs1*^{tmgc1}/*Rs1*^{tmgc1} and *Rs1*^{tmgc1}/Y; formerly *Rs1h*^{tmgc1}) mice were obtained from the Tennessee Mouse Genome Consortium (TMGC) ENU mutagenesis project. These mice are on a mixed genetic background of C57BL/6J (B6) and C3Sn.BLiA-*Pde6b*$^{+}$ (C3H) (Jablonski *et al.* 2005a,b). No gender-specific differences in the retinal phenotype were found among *Rs1* mutant mice. Wild-type AKR/J (AKR) mice and B6(Cg)-*Tyr*$^{c-2J}$/J (B6-*Tyr*$^{c-2J}$/*Tyr*$^{c-2J}$) mice were obtained from The Jackson Laboratory (Bar Harbor, ME). The F_2 intercross and congenic mouse lines were generated as previously described (Johnson *et al.* 2008) and the F_2 mice were further intercrossed to collect more recombinants within the *Mor1* critical region at the F_3 generation. To generate progeny test lines, (AKR × 44TNJ) *Rs1*^{tmgc1}/+ or (AKR × 44TNJ) *Rs1*^{tmgc1}/Y F_2 or F_3 progeny that harbored a crossover event in the *Mor1* minimal genetic region between markers D7Mit279 (83.6Mb) and D7Mit237 (123.0Mb) were mated to (AKR × 44TNJ) *Rs1*^{tmgc1}/+ or (AKR × 44TNJ) *Rs1*^{tmgc1}/Y F_2 progeny that did not contain a crossover event in the *Mor1* critical region. All simple sequence length polymorphisms (SSLPs) and single-nucleotide polymorphisms (SNPs) used as markers in this study were able to distinguish the AKR allele from B6 and C3H alleles. All marker positions reported are based on the NCBI mouse genome build 37.1 reference assembly.

Histological analysis: Histological analysis was performed as previously described (Johnson *et al.* 2008). Following asphyxiation by CO_2 administration, eyes were immediately removed and immersion fixed in Bouin's fixative overnight at 4°. Eyes were then rinsed, dehydrated, and embedded in paraffin. Paraffin blocks were sectioned 6 μm thick on an RM 2135 microtome (Leica Microsystems, Wetzlar, Germany) and mounted on glass slides. The slides were then stained with hematoxylin and eosin (H&E) to visualize the retinal structure for phenotyping. H&E-stained sections were imaged on an Eclipse E600 microscope (Nikon, Tokyo), using a SPOT camera (Spot Diagnostics, Sterling Heights, MI).

Phenotyping by histological analysis: All progeny test animals were phenotyped by histological analysis irrespective of genotyping. Animals were scored for schisis severity in a semiquantitative fashion. Scores ranged from 0 to 2 (from no schisis to severe schisis, respectively). Within each progeny test line, the phenotypic distribution of the progeny haplotypes was compared using one-way analysis of variance (ANOVA) with Bonferroni correction in GraphPad Prism software (GraphPad Software, La Jolla, CA).

Immunohistochemistry: For immunohistochemistry on cryostat sections, 12-μm-thick sections were blocked in PBS with 0.5% Triton X-100 and 2% normal donkey serum for 20 min at room temperature. Next, sections were incubated at 4° overnight in primary antibody solution. Primary antibodies used were PKCα (Sigma, St. Louis), PSD95 (NeuroMab), and GFAP (Thermo Scientific). Sections were rinsed in PBS and incubated in a 1:400 diluted secondary antibody:block solution for 45 min at room temperature. Antibody control slides were made by omitting primary antibody (data not shown). Slides were imaged on a Zeiss 510 confocal laser scanning system and an Axio Imager microscope using LSM 510 software (release 4.2) (Carl Zeiss MicroImaging, Thornwood, NY).

Fluorescence signal quantification: The percentage of GFAP-labeled area occurring below the ganglion cell and nerve fiber layers in sections immunostained with the GFAP antibody was quantified using the histogram function of ImageJ software (available at http://rsb.info.nih.gov/ij; developed by Wayne Rasband, National Institutes of Health, Bethesda, MD) (Vidal *et al.* 2010). To eliminate the signal occurring in retinal astrocytes, the ganglion cell and nerve fiber layers were cropped from the green channel of confocal images of B6 wild-type ($n = 3$), *Rs1*^{tmgc1}/Y *Tyr*$^{+}$/*Tyr*$^{+}$ or *Rs1*^{tmgc1}/Y *Tyr*$^{c-2J}$/*Tyr*$^{+}$ (*Rs1*^{tmgc1}/Y control; $n = 6$), and *Rs1*^{tmgc1}/Y *Tyr*$^{c-2J}$/*Tyr*$^{c-2J}$ ($n = 5$) mice. The percentage of GFAP-labeled area was quantified using the histogram function of ImageJ.

Quantification of ectopic dendrite: Frequencies of ectopically localized bipolar cell dendrites extending into the ONL were quantified in sections immunostained with the PKCα antibody, using the Measure and Label function of ImageJ software (available at http://rsb.info.nih.gov/ij; developed by Wayne Rasband, National Institutes of Health). Total retina length was measured along the outer plexiform layer (OPL), using the Measure function of ImageJ software. Frequency was calculated as the number of ectopic bipolar cell dendrites per millimeter of retina length for B6 wild-type ($n = 5$), *Rs1*^{tmgc1}/Y control ($n = 4$), and *Rs1*^{tmgc1}/Y *Tyr*$^{c-2J}$/*Tyr*$^{c-2J}$ ($n = 4$) mice.

RESULTS

Fine mapping the *Mor1* modifier: Homozygosity for the protective AKR allele of *Mor1* rescues the schisis phenotype in *Rs1*^{tmgc1} mutant mice. The *Mor1* modifier was previously mapped to an estimated genetic distance of 9 cM between the markers D7Mit279 (83.6Mb) and D7Mit237 (123Mb) on mouse Chr 7, using 270 F_2 ani-

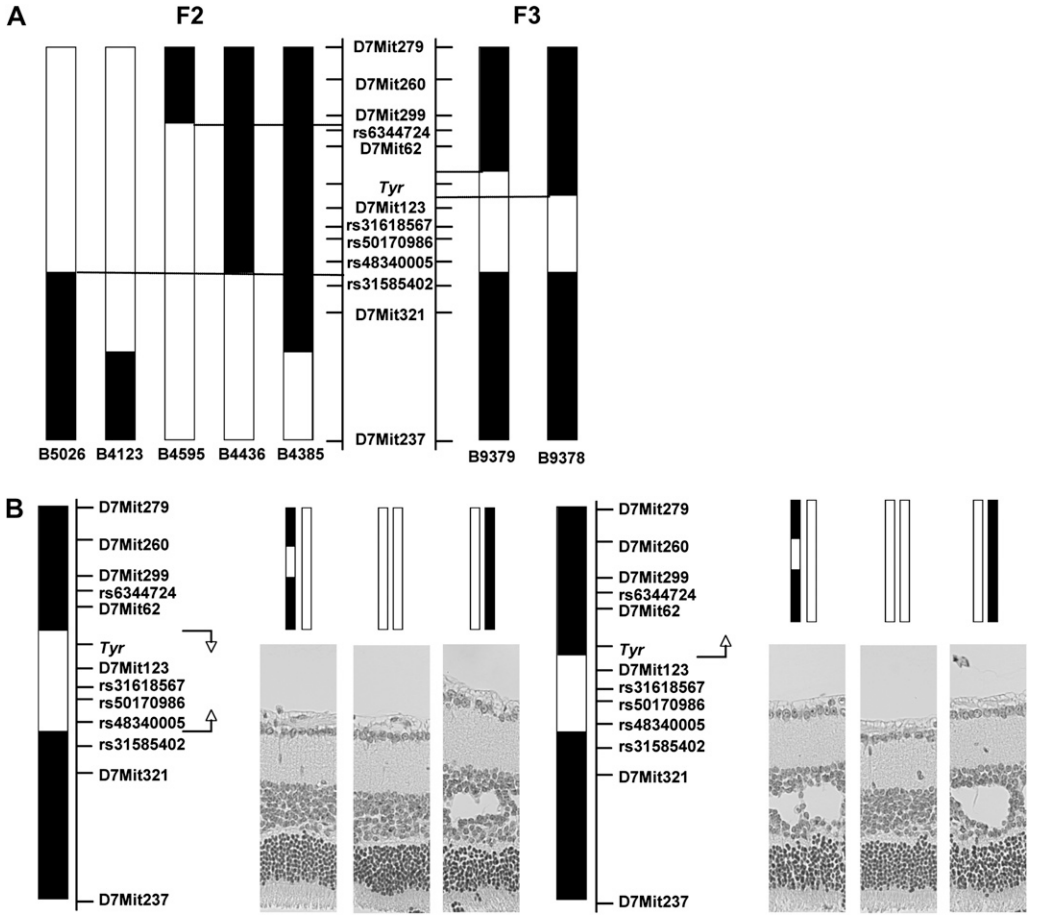

FIGURE 1.—Genetic refinement of the *Mor1* locus. (A) Critical recombinant chromosomes obtained in F_2 (left) and F_3 (right) mice used for progeny testing. Marker positions are indicated between F_2 and F_3 chromosomes. (B) Progeny testing for B9378 and B9379 that define the new *Mor1* minimal genetic region. For both progeny tests, progeny that are homozygous for AKR across Chr 7 do not have schisis (rescued) and progeny that are heterozygous across Chr 7 have schisis (affected). Recombinant progeny from B9379 (left) do not have schisis, while recombinant progeny derived from B9378 (right) have schisis. Therefore *Mor1* is located within the new minimal genetic region flanked by markers D7Mit62 and D7Mit123.

mals (JOHNSON *et al.* 2008). After defining the *Mor1* genetic region, we examined 311 additional (AKR × 44TNJ) F_2 mice for recombination events within the *Mor1* genetic region. Of the 311 mice, 19 were recombinant and were saved for further study.

We used SSLP and SNP markers located in the *Mor1* genetic region to further define the location of crossover events in the 19 recombinant mice (Figure 1). The tyrosinase (*Tyr*) gene is within the minimal genetic region (at 94.6 Mb) and also served as a useful marker (Figure 1). The AKR strain is homozygous for a recessive mutation in the *Tyr* gene (Tyr^c). Therefore, all F_2 mice that are homozygous for the AKR alleles of the *Tyr* locus are albino and have nonpigmented eyes, while F_2 mice that carry at least one 44TNJ allele of the *Tyr* locus have pigmented eyes. Using these additional markers, the locations of crossover events in F_2 recombinant mice were determined (Figure 1A, left). To confirm the genetic region indicated by crossover events in the recombinant animals, progeny testing was performed, which defined the minimal genetic region of *Mor1* flanked by markers D7Mit299 and rs31585402.

We further intercrossed F_2 mice to collect additional recombinants within the *Mor1* critical region at the F_3 generation. For two F_3 mice (B9378 and B9379) with recombination events between D7Mit299 and rs31585402 (Figure 1A, right), progeny testing was performed (Figure 1B). For both progeny tests, progeny that were homozygous for AKR across the *Mor1* locus did not have schisis (rescued) and progeny that were heterozygous across the *Mor1* locus did have schisis (affected). In the progeny line of B9378 (Figure 1B, right), the progeny carrying the recombinant chromosome have schisis and are significantly different in phenotype from nonaffected mice (ANOVA, $P < 0.001$). In the progeny line of B9379 (Figure 1B, left), the progeny carrying the recombinant chromosome do not have schisis and are significantly different in phenotype from affected mice (ANOVA, $P < 0.001$). On the basis of these results, the minimal genetic region of *Mor1* is between markers D7Mit62 and D7Mit123. This region is 4.4 Mb in length and contains 27 genes (supporting information, Table S1).

Tyrosinase as a candidate gene for *Mor1*: As discussed above, the genetic minimal region for the *Mor1* locus contains the *Tyr* gene that is mutated and causes albino phenotypes in AKR mice. To test whether the genetic difference in the *Tyr* gene alone affects the schisis phenotype in $Rs1^{tmgc1}$ mice, we generated $Rs1^{tmgc1}$ mice homozygous for a *Tyr* mutation. We crossed female B6-$Tyr^{c\text{-}2J}/Tyr^{c\text{-}2J}$ albino mice (LE FUR *et al.* 1996) with male $Rs1^{tmgc1}$/Y mice. F_1 mice were intercrossed to generate $Rs1^{tmgc1}$/Y $Tyr^{c\text{-}2J}/Tyr^{c\text{-}2J}$ mice. Since the $Tyr^{c\text{-}2J}$

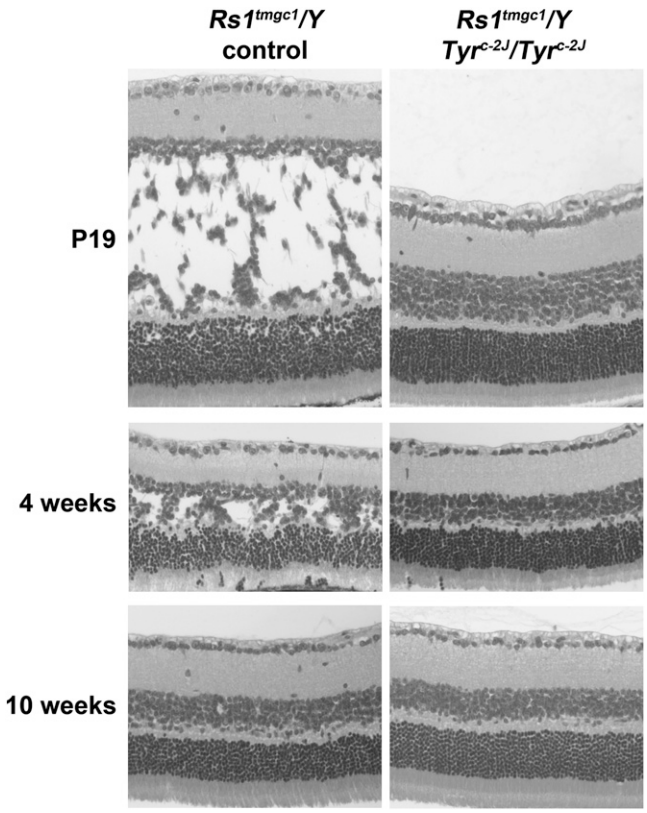

FIGURE 2.—Histological examination of the retina of *Rs1*^{tmgc1} mice with homozygous *Tyr*$^{c-2J}$ mutation. Images are shown of H&E-stained retinal sections from *Rs1*^{tmgc1}/Y control (left) and *Rs1*^{tmgc1}/Y *Tyr*$^{c-2J}$/*Tyr*$^{c-2J}$ (right) mice at P19 (top), 4 weeks (middle), and 16 weeks (bottom) of age. The schisis phenotype is not observed in the *Rs1*^{tmgc1}/Y *Tyr*$^{c-2J}$/*Tyr*$^{c-2J}$ retina throughout the ages examined.

mutation arose on the B6 congenic background (LE FUR *et al.* 1996) and *Rs1*^{tmgc1}/Y mice are on a mixed background of B6 and C3H (JABLONSKI *et al.* 2005a), *Rs1*^{tmgc1}/Y *Tyr*$^{c-2J}$/*Tyr*$^{c-2J}$ mice are expected to carry susceptible B6 or C3H alleles at the *Mor1* locus except for the *Tyr* gene. We observed that the schisis phenotype caused by the *Rs1*^{tmgc1} mutation is rescued in *Rs1*^{tmgc1}/Y *Tyr*$^{c-2J}$/*Tyr*$^{c-2J}$ mice at 4 weeks of age (Figure 2). We also examined the schisis phenotype in these mice at different ages, postnatal day (P) 19 and 10 weeks, and found that it is consistently rescued at all time points tested (Figure 2). The retina of *Rs1*^{tmgc1}/Y *Tyr*$^{c-2J}$/*Tyr*$^{c-2J}$ mice was comparable to that of B6 wild-type mice at all time points examined (data not shown). These results strongly suggest that *Tyr* is the *Mor1* gene.

Effect of the *Tyr*$^{c-2J}$ mutation on other *Rs1* mutant phenotypes: We then tested whether other retinal phenotypes observed in *Rs1* mutant mice are also rescued by the *Tyr*$^{c-2J}$ mutation. It was previously reported that the *Rs1*^{tmgc1} mutation causes ectopic localization of synapses between photoreceptor cells and second-order neurons in the retina (JOHNSON *et al.* 2006). To test if the *Tyr*$^{c-2J}$ mutation affects this synaptic abnormality, we immunostained retinal sections from 4-week-old B6 wild-type ($n = 5$), *Rs1*^{tmgc1}/Y *Tyr*$^{+}$/*Tyr*$^{+}$ or *Rs1*^{tmgc1}/Y *Tyr*$^{c-2J}$/*Tyr*$^{+}$ (*Rs1*^{tmgc1}/Y control; $n = 4$), and *Rs1*^{tmgc1}/Y *Tyr*$^{c-2J}$/*Tyr*$^{c-2J}$ ($n = 4$) mice with the bipolar cell marker, PKCα (Figure 3A). The frequency of ectopic synapses was quantified by counting the number of abnormally extended dendrites. This analysis revealed that the number of ectopic synapses is significantly reduced in *Rs1*^{tmgc1}/Y *Tyr*$^{c-2J}$/*Tyr*$^{c-2J}$ mice compared to *Rs1*^{tmgc1}/Y control mice ($P < 0.001$; Figure 3B).

Abnormal upregulation of intermediate filament protein, GFAP, is another retinal phenotype observed in *Rs1* knockout mice (TAKADA *et al.* 2008). To test whether this phenotype is also observed in *Rs1*^{tmgc1} mice and whether it is rescued by the *Tyr*$^{c-2J}$ mutation, we performed immunohistochemical analysis in 4-week-old B6 wild-type, *Rs1*^{tmgc1}/Y control, and *Rs1*^{tmgc1}/Y *Tyr*$^{c-2J}$/*Tyr*$^{c-2J}$ mice using anti-GFAP antibody. In B6 wild-type mice, the GFAP immunolabeling was restricted to the ganglion cell and nerve fiber layers where astrocytes are localized (Figure 4A, left), whereas it extended across the entire retinal layers in *Rs1*^{tmgc1}/Y mice (Figure 4A, center). In *Rs1*^{tmgc1}/Y *Tyr*$^{c-2J}$/*Tyr*$^{c-2J}$ mice, extension of anti-GFAP labeling is much reduced compared to that in *Rs1*^{tmgc1}/Y mice and reaches only the inner plexiform layer (IPL). Quantification of the GFAP fluorescent signals in the retina excluding the ganglion cell and nerve fiber layers revealed that, while they are significantly increased in *Rs1*^{tmgc1}/Y mice compared to B6 wild-type mice, they are not statistically different between B6 wild-type and *Rs1*^{tmgc1}/Y *Tyr*$^{c-2J}$/*Tyr*$^{c-2J}$ mice (Figure 4B). These results indicate that the *Tyr*$^{c-2J}$ mutation significantly reduces upregulation of GFAP caused by the *Rs1*^{tmgc1} mutation ($P < 0.05$).

GFAP immunoreactivity in the older *Rs1*^{tmgc1} retina: Our previous study on *Rs1*^{tmgc1} mice (JOHNSON *et al.* 2008) and a study using a null mutant for *Rs1* (KJELLSTROM *et al.* 2007) showed that the schisis phenotype caused by the *Rs1* mutation is rescued as mice age. To test whether downregulation of GFAP also occurs in age-associated rescue of schisis, we performed immunostaining of the retina from *Rs1*^{tmgc1}/Y and B6 wild-type mice, using the GFAP antibody at 4 and 16 weeks of age. Despite the rescue of schisis in *Rs1*^{tmgc1}/Y mice at 16 weeks of age (Figure 5A, bottom right), the GFAP immunoreactivity extended across the retinal layers (Figure 5A, top right) as observed at 4 weeks of age (Figure 5A, top left). Quantification of GFAP signals in the retina excluding the ganglion cell and nerve fiber layers revealed that they are not statistically different from those in 4-week-old *Rs1*^{tmgc1}/Y mice ($P = 0.1894$; Figure 5B).

DISCUSSION

We demonstrated here that the mutation in the *Tyr* gene rescues the schisis phenotype caused by the *Rs1*^{tmgc1} mutation in a recessive manner. This finding is consistent

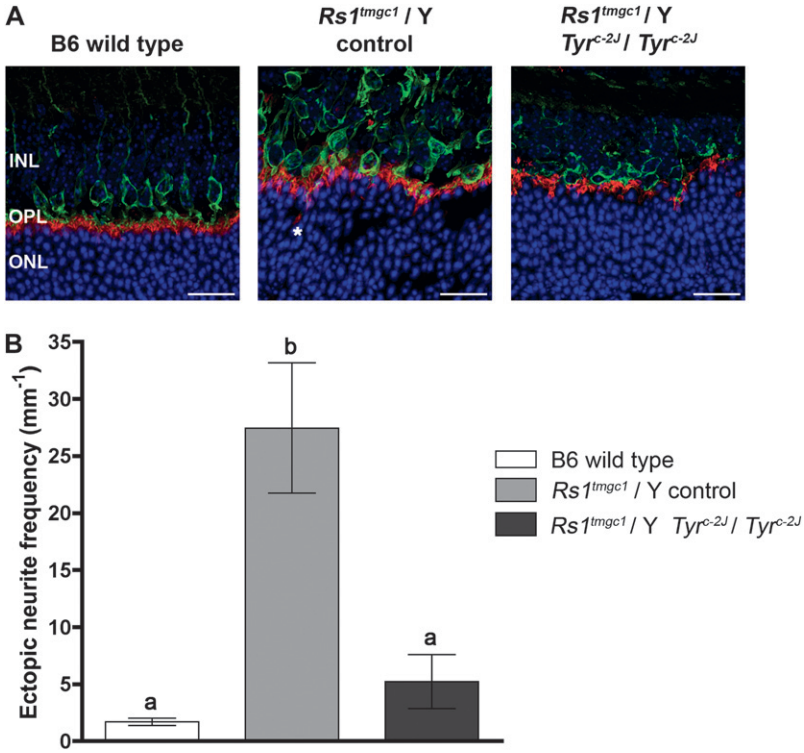

FIGURE 3.—Rescue of ectopic synaptic localization by the *Tyr^{c-2J}* mutation. PKCα-labeled (green) bipolar cell dendrites and PSD95-labeled (red) photoreceptor synaptic terminals are localized in the outer plexiform layer (OPL) in B6 wild-type mice (A, left), while they are ectopically localized in the outer nuclear layer (ONL) in the *Rs1^{tmgc1}*/Y control retina (A, center; asterisk). In the retina of *Rs1^{tmgc1}*/Y *Tyr^{c-2J}*/*Tyr^{c-2J}* mice (A, right), the frequency of ectopically localized synapses is not statistically different from that in the B6 wild-type retina (B). Bar, 20 μm. Error bars represent SEM. Values with different superscripts differ with statistical significance ($P < 0.05$). INL, inner nuclear layer.

with the result of our previous genetic mapping of the modifier of retinoschisis, where the AKR allele of the *Mor1* locus can rescue the schisis phenotype caused by the *Rs1^{tmgc1}* mutation in a recessive manner (JOHNSON *et al.* 2008). We continued fine mapping of the *Mor1* locus and found that the minimal region contained 27 genes including *Tyr*. To test *Tyr* as a candidate gene for *Mor1*, we took advantage of the availability of the *Tyr^{c-2J}* mutation on the B6 background and tested its effect on the schisis phenotype. Upon studying the time course of the schisis phenotype, we found that it is rescued by the *Tyr^{c-2J}* mutation throughout the ages examined. Thus, the present study strongly suggests that *Tyr* is the *Mor1* gene.

It was previously reported that ectopic localization of synapses between photoreceptor cells and secondary neurons is caused by the *Rs1^{tmgc1}* (JOHNSON *et al.* 2006) and *Rs1* null (TAKADA *et al.* 2008) mutations. In this study, we showed that the *Tyr^{c-2J}* mutation also rescues this synaptic abnormality in *Rs1^{tmgc1}* mice. Since this synaptic abnormality is concurrently observed with aberrant synaptic transmission in a number of mouse models (DICK *et al.* 2003; HAESELEER *et al.* 2004; MANSERGH *et al.* 2005; MORGANS *et al.* 2005; CHANG *et al.* 2006; JOHNSON *et al.* 2006; TAKADA *et al.* 2008), it would be ideal to test whether the *Tyr^{c-2J}* mutation also rescues the synaptic transmission defect. However, because of the difference in ERG patterns between albino and pigmented mice (PINTO *et al.* 2007), it was not appropriate to compare the ERG between *Rs1^{tmgc1}*/Y control (pigmented) and *Rs1^{tmgc1}*/Y *Tyr^{c-2J}*/*Tyr^{c-2J}* (albino) mice.

We also demonstrated that upregulation and extension of GFAP immunoreactivity across the retinal layers is observed in *Rs1^{tmgc1}* mice and that this phenotype is also rescued by the *Tyr^{c-2J}* mutation. The upregulation and extension of GFAP immunoreactivity was previously reported in *Rs1* null mutant mice (TAKADA *et al.* 2008). Upregulation of GFAP in retinal Müller cells is considered an indicator of stress in the retina and can be observed in a number of retinal degenerative conditions and retinal injuries (LEWIS and FISHER 2003). Therefore, the decreased level of GFAP immunoreactivity in *Rs1^{tmgc1}*/Y *Tyr^{c-2J}*/*Tyr^{c-2J}* mice also indicates that the modifier gene decreases the retinal stress in *Rs1^{tmgc1}*/Y mice. We previously reported that the schisis phenotype is rescued in *Rs1^{tmgc1}* mice as the mice age (JOHNSON *et al.* 2008). However, in 16-week-old *Rs1^{tmgc1}* mice, GFAP signals are still increased despite that schisis is no longer observed in *Rs1^{tmgc1}*/Y mice at this age. This observation suggests that the upregulation of GFAP in *Rs1^{tmgc1}*/Ymice may not be the result of physical changes associated with schisis but may rather occur due to other abnormalities caused by the *Rs1* mutation, which appear to be rescued by the *Tyr^{c-2J}* mutation but not by age-associated changes.

Taken together, our current study suggests that the modifier gene, *Tyr*, could rescue multiple retinal abnormalities caused by the *Rs1* mutation. This brings us to the next question: What is the molecular mechanism underlying the rescue of *Rs1* mutant phenotypes by the *Tyr* mutation? Two major hypotheses are currently being considered. The first hypothesis is that the *Tyr* mutation affects the level of the middle product of melanin

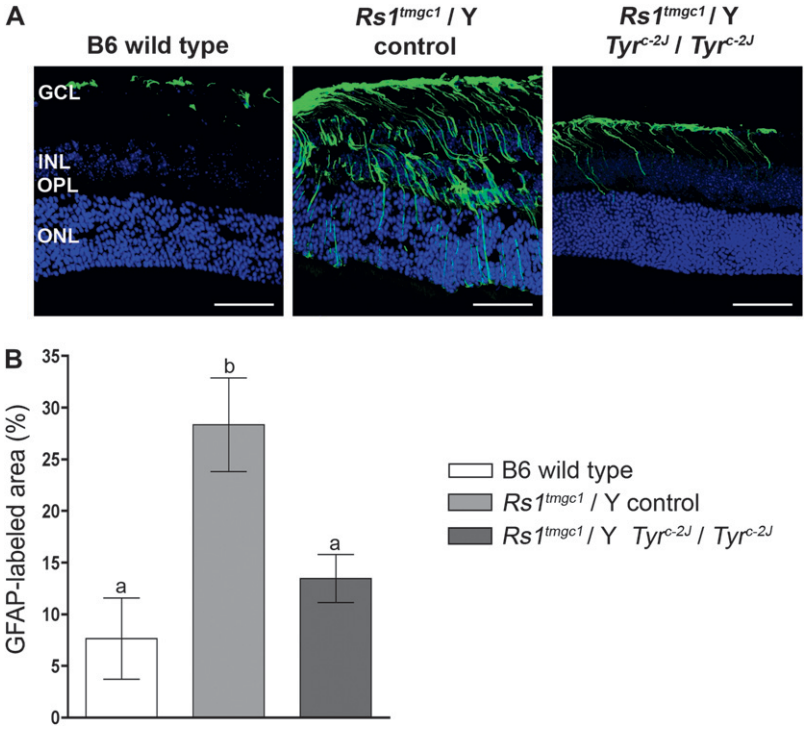

FIGURE 4.—GFAP upregulation in the retina of *Rs1*^{tmgc1} mice and its rescue by the *Tyr*$^{c-2J}$ mutation. (A) Immunohistochemistry for GFAP. While GFAP expression is observed only in the ganglion cell and nerve fiber layers in 4-week-old B6 wild-type mice (A, left), it extends across the retinal layers and reaches the outer nuclear layer (ONL) in the *Rs1*^{tmgc1}/Y control retina (A, center). In the retina of *Rs1*^{tmgc1}/Y *Tyr*$^{c-2J}$/ *Tyr*$^{c-2J}$ mice, upregulation and extension of GFAP signals are much reduced (A, right). (B) Quantification of GFAP immunostained area in the retina excluding the ganglion cell and nerve fiber layers. The level of GFAP signals in the *Rs1*^{tmgc1}/Y *Tyr*$^{c-2J}$/*Tyr*$^{c-2J}$ retina is not significantly different from that in the B6 control retina. Bar, 50 μm. GCL, ganglion cell layer; INL, inner nuclear layer; OPL, outer plexiform layer.

synthesis that may in turn affect the retinal phenotypes. Tyrosinase is a key enzyme in pigment synthesis and produced in retinal pigment epithelial (RPE) cells that are adjacent to the sensory retina. It catalyzes conversion of tyrosine to L-dopa and L-dopa to dopaquinone (ITO 2003). It has been postulated that the middle product, L-dopa, is released from RPE cells into the extracellular space (PAGE-MCCAW *et al.* 2004). L-dopa is known to affect retinal development and function (KUBRUSLY *et al.* 2003; TIBBER *et al.* 2006), and it is also the precursor of dopamine, a neurotransmitter produced by dopaminergic neurons that has roles in retinal development and function as well (REIS *et al.* 2007). Thus, the *Tyr* mutation may decrease the concentration of L-dopa and dopamine in the retina, which may in turn affect *Rs1* mutant phenotypes in the retina. A similar scenario was revealed for the modification of ocular defects in mouse models of primary congenital glaucoma (PCG). In theses models, the *Tyr* mutation was shown to increase the severity of the ocular drainage structure defects associated with PCG (LIBBY *et al.* 2003). Administration of L-dopa was found to prevent this modification of abnormalities (LIBBY *et al.* 2003), indicating that the *Tyr* mutation modifies the severity of PCG phenotypes by affecting L-dopa levels. Alternatively, modifier effects of the *Tyr* mutation on retinoschisis may be associated with pigmentation. It is known that albino animals receive a 90-fold higher intensity of light on their retina compared to pigmented species (LYUBARSKY *et al.* 2004), which could potentially cause alteration in

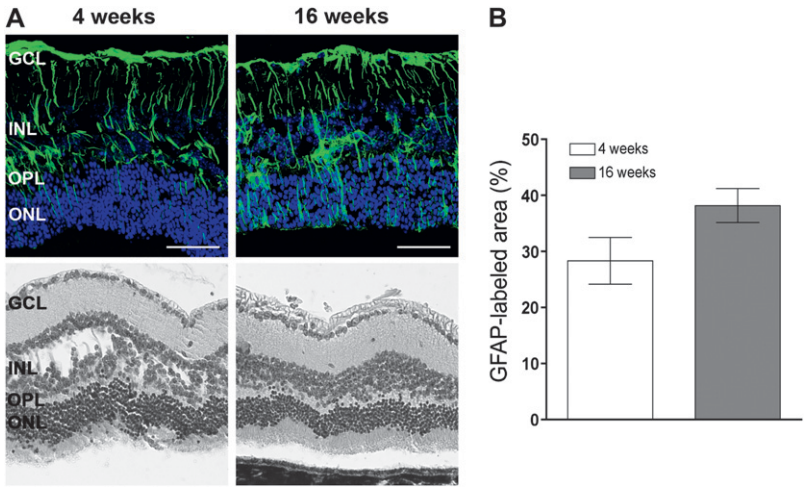

FIGURE 5.—GFAP expression in the older *Rs1*^{tmgc1} mice. (A) Immunohistochemistry for GFAP in the retinas of 4-week-old (left, top) and 16-week-old (right, top) *Rs1*^{tmgc1} mice. While the schisis phenotype observed at 4 weeks of age (left, bottom) is rescued by 16 weeks of age (right, bottom), GFAP remains upregulated at 16 weeks of age. (B) The percentage of immunolabeled area in the green channel occurring in the retina excluding the ganglion cell and nerve fiber layers in 16-week-old *Rs1*^{tmgc1} retina is not significantly different from that in 4-week-old *Rs1*^{tmgc1} retina. Bar, 50 μm. GCL, ganglion cell layer; INL, inner nuclear layer; OPL, outer plexiform layer; ONL, outer nuclear layer.

the retinal functions. In fact, there are a number of retinal abnormalities reported to be associated with albinism (Oetting 1999; Russell-Eggitt 2001). However, it is interesting to note that, in the case of *Rs1* mutant phenotypes, albinism is correlated with the rescue (improvement) of retinal phenotypes rather than exacerbation of the phenotypes. Further studies are necessary to test these hypotheses and to understand how the phenotypes of retinoschisis are rescued by the homozygous *Tyr* mutation.

This is the first study to identify a genetic factor that affects the severity of retinoschisis caused by the *Rs1* mutation. Our study also indicated that the effect of the *Tyr* mutation is not only on the schisis phenotype but also on other retinal phenotypes such as GFAP upregulation in the Müller cells and ectopic localization of synapses. Our findings suggest a new pathway involving the *Tyr* gene that affects the severity of retinoschisis and may also help us understand the basis of the phenotypic variation in human XLRS patients.

The authors thank Satoshi Kinoshita for generating frozen sections and the University of Wisconsin (Madison, WI) Genetics Confocal Facility for the use of the confocal microscope. This project was supported by grants to A.I. from the National Institutes of Health (R01 EY016394), by the Rebecca Meyer Brown Pilot Project Award Professorship from the Retina Research Foundation, by an Individual Investigator Grant from the Foundation Fighting Blindness, and by a grant to E.E.G. from the National Institutes of Health (R01 EY017841).

LITERATURE CITED

Baumgartner, S., K. Hofmann, R. Chiquet-Ehrismann and P. Bucher, 1998 The discoidin domain family revisited: new members from prokaryotes and a homology-based fold prediction. Protein Sci. **7:** 1626–1631.

Chang, B., J. R. Heckenlively, P. R. Bayley, N. C. Brecha, M. T. Davisson *et al.*, 2006 The nob2 mouse, a null mutation in Cacna1f: anatomical and functional abnormalities in the outer retina and their consequences on ganglion cell visual responses. Vis. Neurosci. **23:** 11–24.

Dick, O., S. tom Dieck, W. D. Altrock, J. Ammermuller, R. Weiler *et al.*, 2003 The presynaptic active zone protein bassoon is essential for photoreceptor ribbon synapse formation in the retina. Neuron **37:** 775–786.

Eksandh, L. C., V. Ponjavic, R. Ayyagari, E. L. Bingham, K. T. Hiriyanna *et al.*, 2000 Phenotypic expression of juvenile X-linked retinoschisis in Swedish families with different mutations in the XLRS1 gene. Arch. Ophthalmol. **118:** 1098–1104.

George, N. D., J. R. Yates and A. T. Moore, 1995 X linked retinoschisis. Br. J. Ophthalmol. **79:** 697–702.

George, N. D., J. R. Yates and A. T. Moore, 1996 Clinical features in affected males with X-linked retinoschisis. Arch. Ophthalmol. **114:** 274–280.

Haeseleer, F., Y. Imanishi, T. Maeda, D. E. Possin, A. Maeda *et al.*, 2004 Essential role of Ca2+-binding protein 4, a Cav1.4 channel regulator, in photoreceptor synaptic function. Nat. Neurosci. **7:** 1079–1087.

Huopaniemi, L., J. Fellman, A. Rantala, A. Eriksson, H. Forsius *et al.*, 1999 Skewed secondary sex ratio in the offspring of carriers of the 214G > A mutation of the RS1 gene. Ann. Hum. Genet. **63:** 521–533.

Ito, S., 2003 The IFPCS presidential lecture: a chemist's view of melanogenesis. Pigment Cell Res. **16:** 230–236.

Jablonski, M. M., C. Dalke, X. Wang, L. Lu, K. F. Manly *et al.*, 2005a An ENU-induced mutation in Rs1h causes disruption of retinal structure and function. Mol. Vis. **11:** 569–581.

Jablonski, M. M., X. Wang, L. Lu, D. R. Miller, E. M. Rinchik *et al.*, 2005b The Tennessee Mouse Genome Consortium: identification of ocular mutants. Vis. Neurosci. **22:** 595–604.

Johnson, B. A., S. Ikeda, L. H. Pinto and A. Ikeda, 2006 Reduced synaptic vesicle density and aberrant synaptic localization caused by a splice site mutation in the Rs1h gene. Vis. Neurosci. **23:** 887–898.

Johnson, B. A., N. Aoyama, N. H. Friedell, S. Ikeda and A. Ikeda, 2008 Genetic modification of the schisis phenotype in a mouse model of X-linked retinoschisis. Genetics **178:** 1785–1794.

Kjellstrom, S., R. A. Bush, Y. Zeng, Y. Takada and P. A. Sieving, 2007 Retinoschisin gene therapy and natural history in the Rs1h-KO mouse: long-term rescue from retinal degeneration. Invest. Ophthalmol. Vis. Sci. **48:** 3837–3845.

Kubrusly, R. C., M. Z. Guimaraes, A. P. Vieira, J. N. Hokoc, D. E. Casarini *et al.*, 2003 L-DOPA supply to the neuro retina activates dopaminergic communication at the early stages of embryonic development. J. Neurochem. **86:** 45–54.

Le Fur, N., S. R. Kelsall and B. Mintz, 1996 Base substitution at different alternative splice donor sites of the tyrosinase gene in murine albinism. Genomics **37:** 245–248.

Lewis, G. P., and S. K. Fisher, 2003 Up-regulation of glial fibrillary acidic protein in response to retinal injury: its potential role in glial remodeling and a comparison to vimentin expression. Int. Rev. Cytol. **230:** 263–290.

Libby, R. T., R. S. Smith, O. V. Savinova, A. Zabaleta, J. E. Martin *et al.*, 2003 Modification of ocular defects in mouse developmental glaucoma models by tyrosinase. Science **299:** 1578–1581.

Lyubarsky, A. L., L. L. Daniele and E. N. Pugh, Jr., 2004 From candelas to photoisomerizations in the mouse eye by rhodopsin bleaching in situ and the light-rearing dependence of the major components of the mouse ERG. Vision Res. **44:** 3235–3251.

Mansergh, F., N. C. Orton, J. P. Vessey, M. R. Lalonde, W. K. Stell *et al.*, 2005 Mutation of the calcium channel gene Cacna1f disrupts calcium signaling, synaptic transmission and cellular organization in mouse retina. Hum. Mol. Genet. **14:** 3035–3046.

Molday, L. L., D. Hicks, C. G. Sauer, B. H. Weber and R. S. Molday, 2001 Expression of X-linked retinoschisis protein RS1 in photoreceptor and bipolar cells. Invest. Ophthalmol. Vis. Sci. **42:** 816–825.

Molday, L. L., W. W. Wu and R. S. Molday, 2007 Retinoschisin (RS1), the protein encoded by the X-linked retinoschisis gene, is anchored to the surface of retinal photoreceptor and bipolar cells through its interactions with a Na/K ATPase-SARM1 complex. J. Biol. Chem **282:** 32792–32801.

Morgans, C. W., P. R. Bayley, N. W. Oesch, G. Ren, L. Akileswaran *et al.*, 2005 Photoreceptor calcium channels: insight from night blindness. Vis. Neurosci. **22:** 561–568.

Oetting, W. S., 1999 Albinism. Curr. Opin. Pediatr. **11:** 565–571.

Page-McCaw, P. S., S. C. Chung, A. Muto, T. Roeser, W. Staub *et al.*, 2004 Retinal network adaptation to bright light requires tyrosinase. Nat. Neurosci. **7:** 1329–1336.

Peachey, N. S., G. A. Fishman, D. J. Derlacki and M. G. Brigell, 1987 Psychophysical and electroretinographic findings in X-linked juvenile retinoschisis. Arch. Ophthalmol. **105:** 513–516.

Pimenides, D., N. D. George, J. R. Yates, K. Bradshaw, S. A. Roberts *et al.*, 2005 X-linked retinoschisis: clinical phenotype and RS1 genotype in 86 UK patients. J. Med. Genet. **42:** e35.

Pinto, L. H., B. Invergo, K. Shimomura, J. S. Takahashi and J. B. Troy, 2007 Interpretation of the mouse electroretinogram. Doc. Ophthalmol. **115:** 127–136.

Reid, S. N., N. B. Akhmedov, N. I. Piriev, C. A. Kozak, M. Danciger *et al.*, 1999 The mouse X-linked juvenile retinoschisis cDNA: expression in photoreceptors. Gene **227:** 257–266.

Reis, R. A., A. L. Ventura, R. C. Kubrusly, M. C. de Mello and F. G. de Mello, 2007 Dopaminergic signaling in the developing retina. Brain Res. Rev. **54:** 181–188.

Retinoschisis Consortium, 1998 Functional implications of the spectrum of mutations found in 234 cases with X-linked juvenile retinoschisis. Hum. Mol. Genet. **7:** 1185–1192.

Russell-Eggitt, I., 2001 Albinism. Ophthalmol. Clin. North Am. **14:** 533–546.

Sauer, C. G., A. Gehrig, R. Warneke-Wittstock, A. Marquardt, C. C. Ewing *et al.*, 1997 Positional cloning of the gene associated with X-linked juvenile retinoschisis. Nat. Genet. **17:** 164–170.

Seiving, P., 1998 Juvenile retinoschisis, pp. 347–356 in *Genetic Diseases of the Eye*, edited by E. Traboulsi. Oxford University Press, New York.

Sergeev, Y. V., R. C. Caruso, M. R. Meltzer, N. Smaoui, I. M. MacDonald *et al.*, 2010 Molecular modeling of retinoschisin with functional analysis of pathogenic mutations from human X-linked retinoschisis. Hum. Mol. Genet. **19:** 1302–1313.

Shi, L., K. Jian, M. L. Ko, D. Trump and G. Y. Ko, 2009 Retinoschisin, a new binding partner for L-type voltage-gated calcium channels in the retina. J. Biol. Chem. **284:** 3966–3975.

Takada, Y., R. N. Fariss, A. Tanikawa, Y. Zeng, D. Carper *et al.*, 2004 A retinal neuronal developmental wave of retinoschisin expression begins in ganglion cells during layer formation. Invest. Ophthalmol. Vis. Sci. **45:** 3302–3312.

Takada, Y., R. N. Fariss, M. Muller, R. A. Bush, E. J. Rushing *et al.*, 2006 Retinoschisin expression and localization in rodent and human pineal and consequences of mouse RS1 gene knockout. Mol. Vis. **12:** 1108–1116.

Takada, Y., C. Vijayasarathy, Y. Zeng, S. Kjellstrom, R. A. Bush *et al.*, 2008 Synaptic pathology in retinoschisis knockout (Rs1-/y) mouse retina and modification by rAAV-Rs1 gene delivery. Invest. Ophthalmol. Vis. Sci. **49:** 3677–3686.

Tibber, M. S., A. V. Whitmore and G. Jeffery, 2006 Cell division and cleavage orientation in the developing retina are regulated by L-DOPA. J. Comp. Neurol. **496:** 369–381.

Vidal, L., F. Diaz, A. Villena, M. Moreno, J. G. Campos *et al.*, 2010 Reaction of Muller cells in an experimental rat model of increased intraocular pressure following timolol, latanoprost and brimonidine. Brain Res. Bull. **82:** 18–24.

Wu, W. W., and R. S. Molday, 2003 Defective discoidin domain structure, subunit assembly, and endoplasmic reticulum processing of retinoschisin are primary mechanisms responsible for X-linked retinoschisis. J. Biol. Chem. **278:** 28139–28146.

Communicating editor: D. W. Threadgill

GENETICS

Supporting Information
http://www.genetics.org/cgi/content/full/genetics.110.120840/DC1

Tyrosinase Is the Modifier of Retinoschisis in Mice

Britt A. Johnson, Brian S. Cole, Eldon E. Geisert, Sakae Ikeda and Akihiro Ikeda

DOI: 10.1534/genetics.110.120840

TABLE S1

Genes located within the *Mor1* minimal genetic region

Start Position (Mb)	Gene Symbol	Gene Name	Molecular Function/Biological Process
92004875	Olfr291	olfactory receptor 291	sensory perception of smell, G-protein coupled receptor activity, olfactory receptor activity, signal transducer activity
92064291	Olfr290	olfactory receptor 290	sensory perception of smell, G-protein coupled receptor activity, olfactory receptor activity, signal transducer activity
92091667	Vmn2r65	vomeronasal 2, receptor 65	receptor activity, signal transduction
92154952	Vmn2r66	vomeronasal 2 receptor o (Fragment)	(no biological data available)
93417299	Olfr310	olfactory receptor 310	sensory perception of smell, G-protein coupled receptor activity, olfactory receptor activity, signal transducer activity
93454695	Olfr309	olfactory receptor 309	sensory perception of smell, G-protein coupled receptor activity, olfactory receptor activity, signal transducer activity
93469534	Olfr308	olfactory receptor 308	sensory perception of smell, G-protein coupled receptor activity, olfactory receptor activity, signal transducer activity
93483963	Olfr307	olfactory receptor 307	sensory perception of smell, G-protein coupled receptor activity, olfactory receptor activity, signal transducer activity
93511886	Olfr305	olfactory receptor 305	sensory perception of smell, G-protein coupled receptor activity, olfactory receptor activity, signal transducer activity
93534167	Olfr304	olfactory receptor 304	sensory perception of smell, G-protein coupled receptor activity, olfactory receptor activity, signal transducer activity
93543047	Olfr303	olfactory receptor 303	sensory perception of smell, G-protein coupled receptor activity, olfactory receptor activity, signal transducer activity
93560871	Olfr301	olfactory receptor 301	sensory perception of smell, G-protein coupled receptor activity, olfactory receptor activity, signal transducer activity
93613923	Olfr299	olfactory receptor 299	sensory perception of smell, G-protein coupled receptor activity, olfactory receptor activity, signal transducer activity
93637061	Olfr298	olfactory receptor 298	sensory perception of smell, G-protein coupled receptor activity, olfactory receptor activity, signal transducer activity
93675269	Olfr297	olfactory receptor 297	sensory perception of smell, G-protein coupled receptor activity, olfactory receptor activity, signal transducer activity
93733787	Olfr295	olfactory receptor 295	sensory perception of smell, G-protein coupled receptor activity, olfactory receptor activity, signal transducer activity
93764146	Olfr294	olfactory receptor 294	sensory perception of smell, G-protein coupled receptor activity, olfactory receptor activity, signal transducer activity
93812174	Olfr293	olfactory receptor 293	sensory perception of smell, G-protein coupled receptor activity, olfactory receptor activity, signal transducer activity
93836851	Olfr292	olfactory receptor 292	sensory perception of smell, G-protein coupled receptor activity, olfactory

			receptor activity, signal transducer activity
93867497	Folh1	folate hydrolase	folic acid and derivative metabolic process, glutamate carboxypeptidase II activity, membrane dipeptidase activity, gamma-glutamyl hydrolase activity
93943660	Vmn2r77	vomeronasal receptor	(no biological data available)
94395308	Nox4	NADPH oxidase 4	bone resorption, superoxide-generating NADPH oxidase activity, negative regulation of cell proliferation, iron ion binding
94575915	Tyr	tyrosinase	melanin biosynthetic process, pigmentation, oxidoreductase activity, monophenol monooxygenase activity, copper ion binding
94750952	Grm5	glutamate receptor, metabotropic 5	G-protein coupled receptor protein signaling pathway, learning, locomotor behavior, regulation of long-term neuronal synaptic plasticity
95426645	Ctsc	cathepsin C	cysteine-type endopeptidase activity, dipeptidyl-peptidase I activity, chloride ion binding, peptidase activity
95578783	RAB38	Rab38, member of RAS oncogene family	small GTPase mediated signal transduction, GTP binding, protein binding
95678953	Rps13	ribosomal protein S13	structural constituent of ribosome, RNA binding, translation

Gene symbols and the start position on Chr 7 in megabases (Mb) are given for each gene.